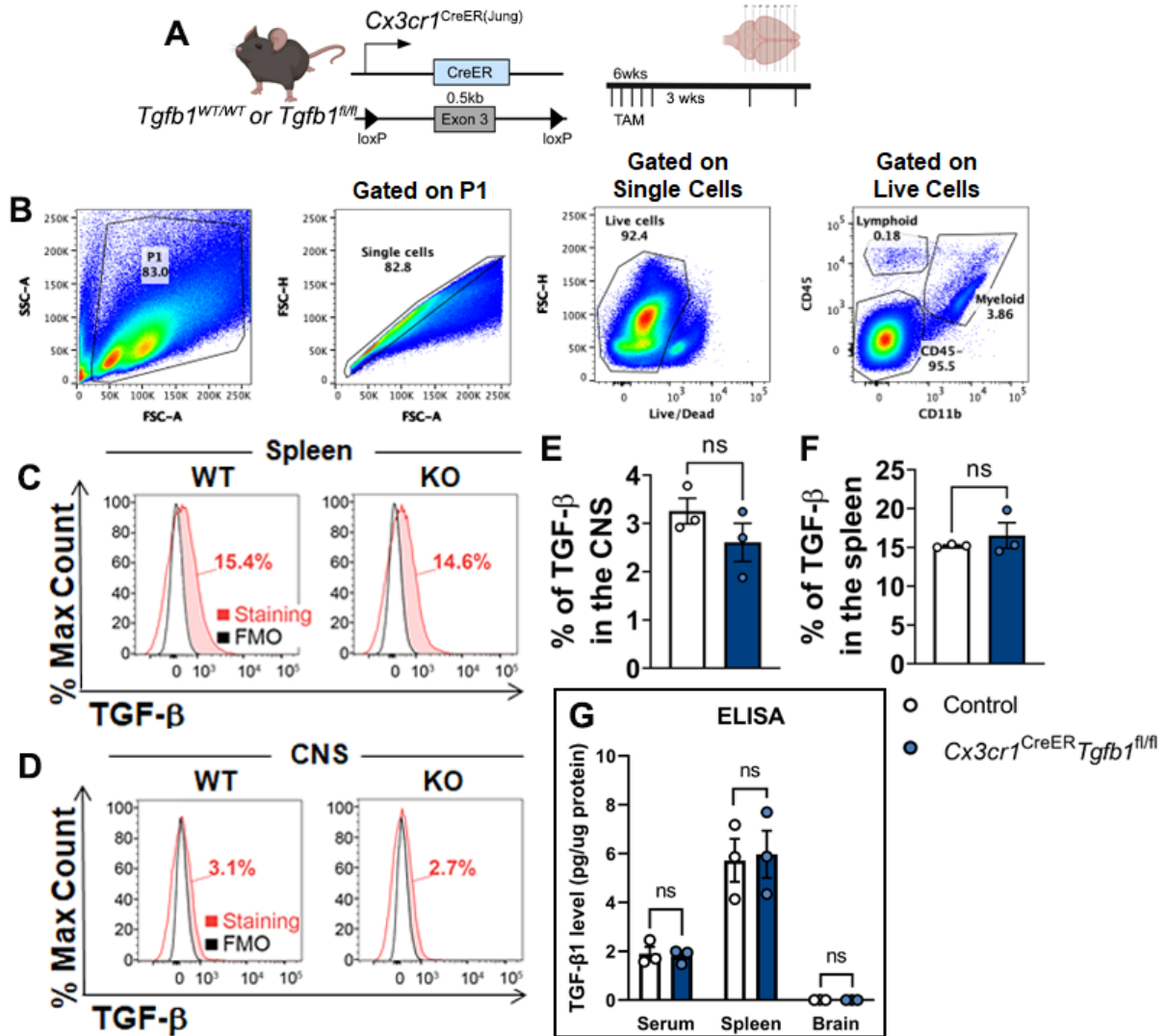
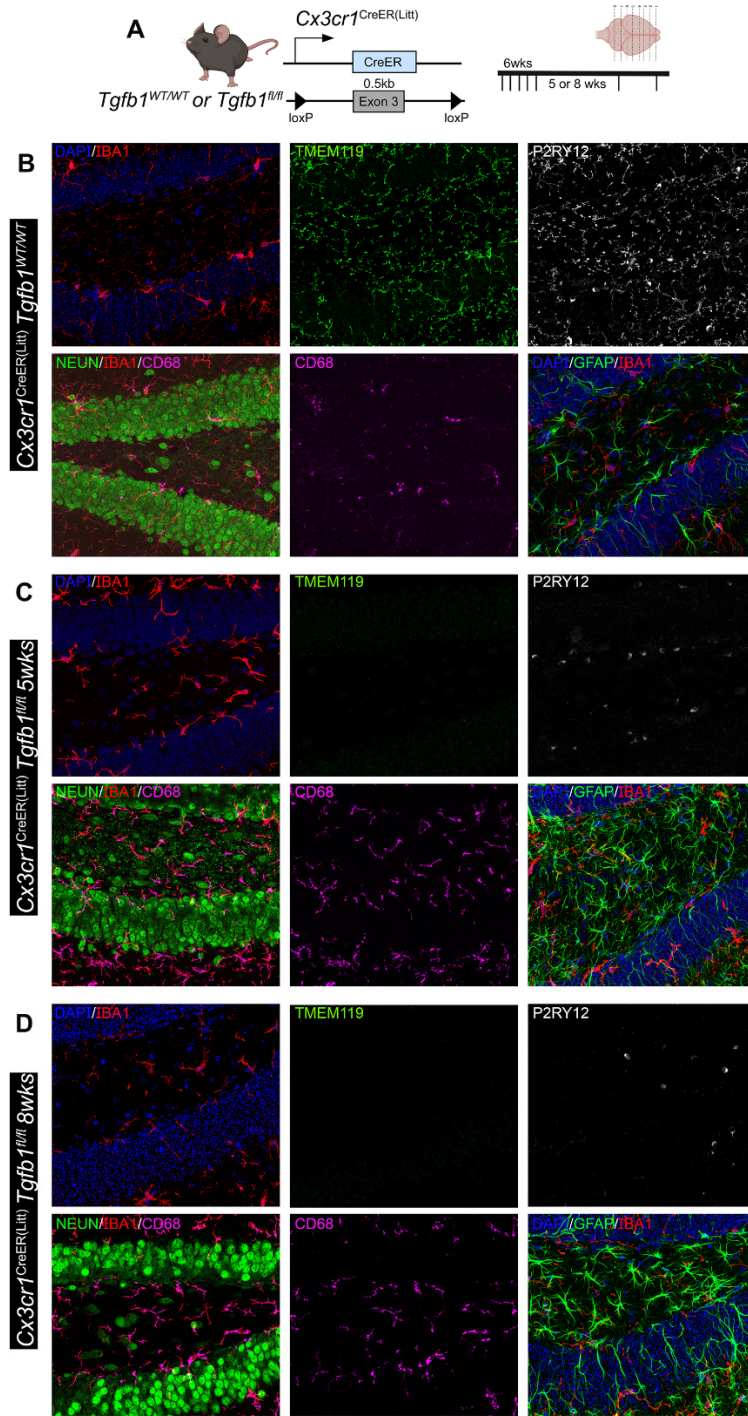


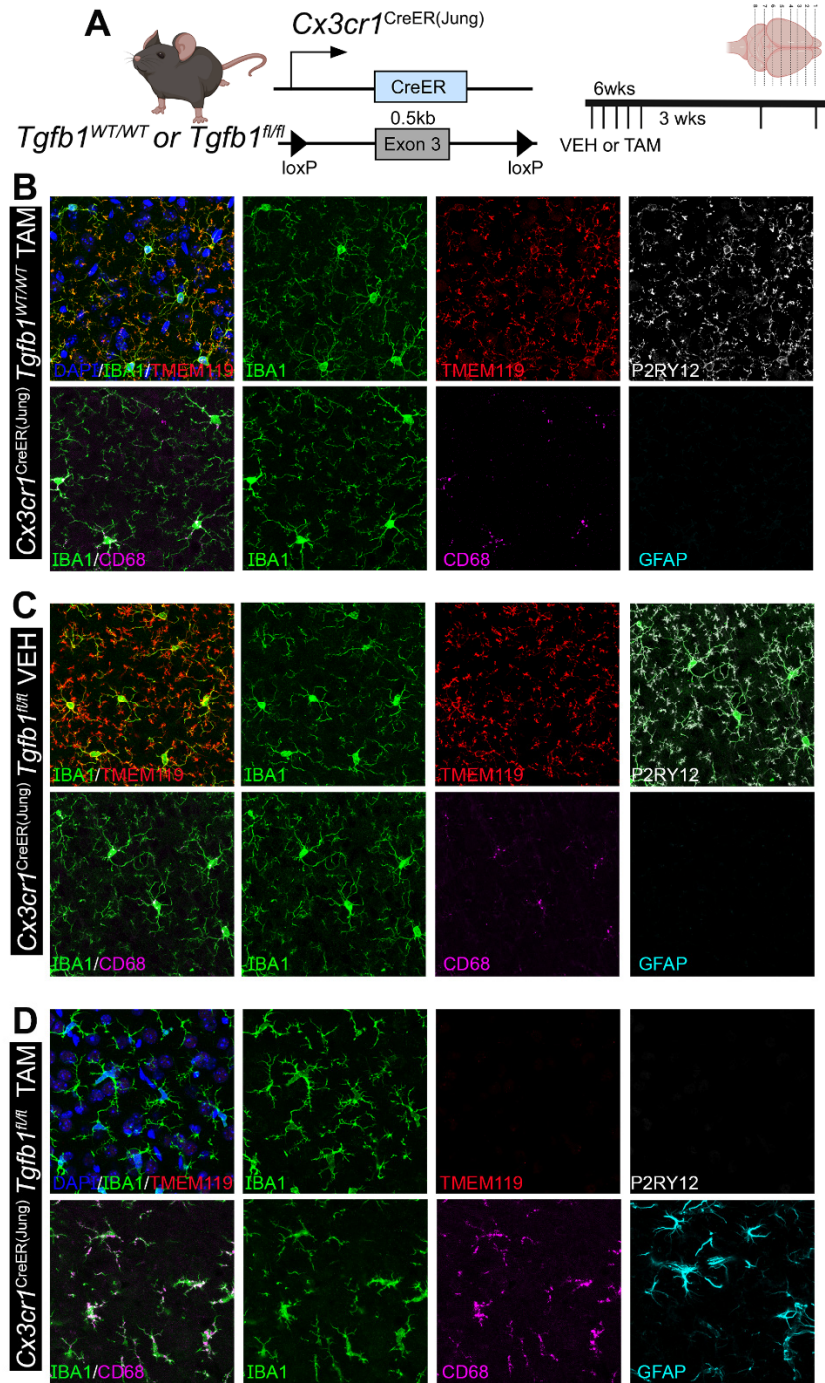
Supplementary Figure 1. *Tgfb1* gene expression is enriched in microglia in adult mouse brains. (A, B) Publicly available single-cell RNA-sequencing showing microglial enrichment for *Tgfb1* expression from Zhang et. al 2014 (A) showing fragments per kilobase of transcript per million reads mapped (FPKM) and a second independent Single-cell portal data set¹ (B) showing similar microglial enrichment of the *Tgfb1* expression among different cell types. (C) Representative images using combined RNA-scope/Immunohistochemistry visualizing RNA-scope in situ signal for *Tgfb1* mRNA and *Tgfb1* (*Alk5*) mRNA combined with IHC for IBA1 and NEUN showing colocalization of *Tgfb1* and *Alk5* mRNA with IBA1+ microglia (white arrow) but not in NEUN+ neurons (white arrowhead). Note some *Tgfb1* mRNA signals in IBA1-cells (yellow arrowhead). (D) Experimental timeline for PLX5562 ablation of microglia, (E) microglia ablation leads to a significant decrease of *Iba1*, *Tgfb1*, and *Alk5* mRNA levels (normalized to Hmbs). Mean±SE, ** = p<0.001, *** = p<0.0005, **** = P<0.0001, Student's t-test (each data point represents an individual animal).



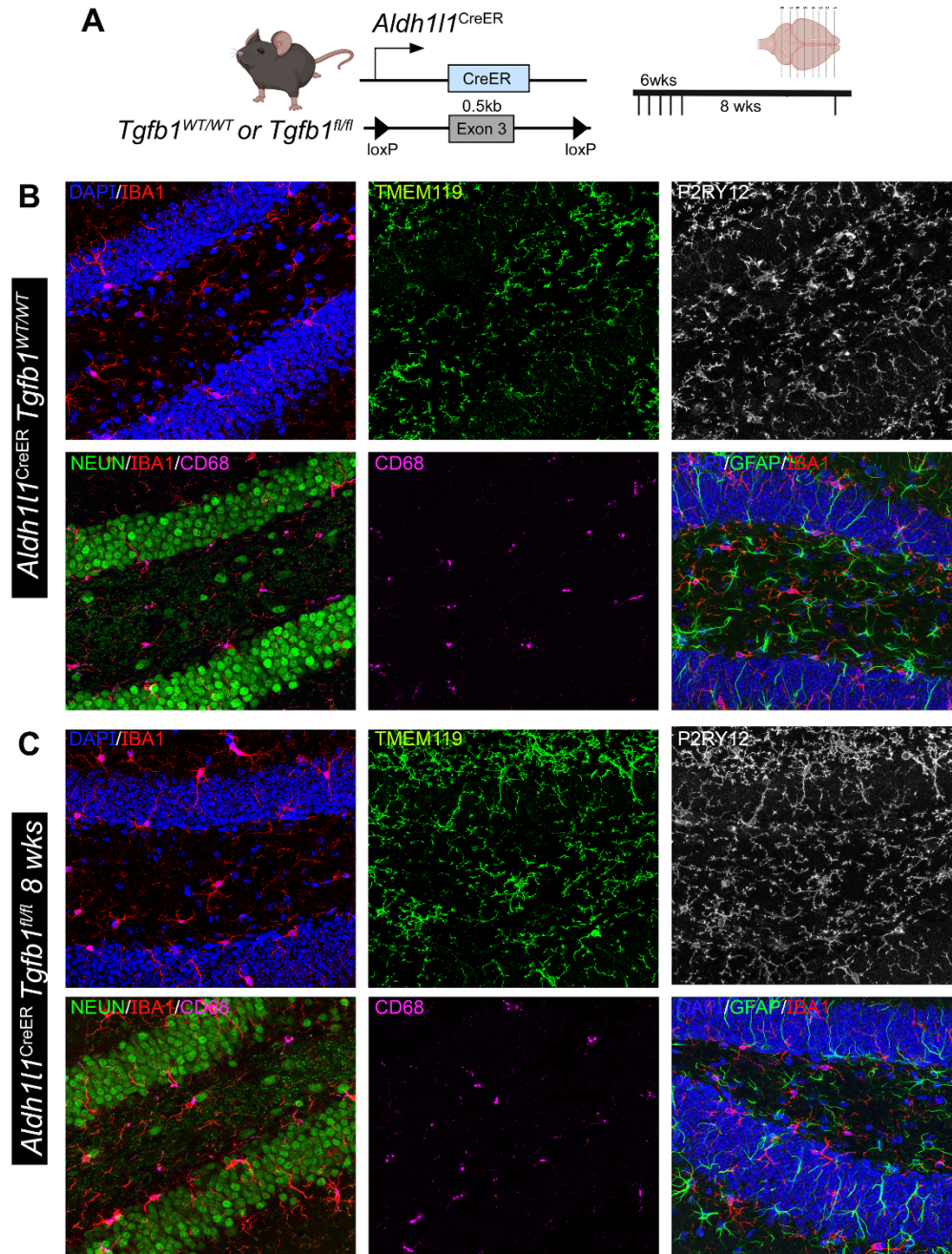
Supplementary Figure 2. FACS or ELISA detection of TGF-β1 protein in the brain, serum, and spleen in WT or MG-*Tgfb1* iKO mice. (A) Timeline for using *Cx3cr1*^{CreER} driver to target myeloid cell inducible *Tgfb1* loss (samples were harvested at 3 weeks post TAM). (B) Gating strategy for identifying the myeloid cells in single-cell suspension. Cells were first gated according to FSC-SSC, then restricted to singles cells and live cells. Myeloid cells were identified as CD45⁺ CD11b⁺. (C, D) FACS analyses of TGF-β expression by myeloid cells in the spleen (top histograms) and in the CNS (lower histograms). The fluorescence minus one (FMO) is represented in black histograms and TGF-β immunostaining is shown in red. TGF-β staining above the background (FMO) is shown in solid red and represents the percentage shown for each analysis. (E, F) Compilation of TGF-β expression by flow cytometry on myeloid cells from the spleen and CNS of WT and KO mice. (G) ELISA quantification (pg/μg total protein) from serum and tissue from the spleen and brain (n = 3 mice per group) showing no difference in TGF-β protein levels in serum or spleen of *Cx3cr1*^{CreER}-*tgfb1* iKO or control mice and that the brain TGF-β ligand levels are below the detection limit of the kit. Mean±SE, Student's t-test (each data point represents a single animal).



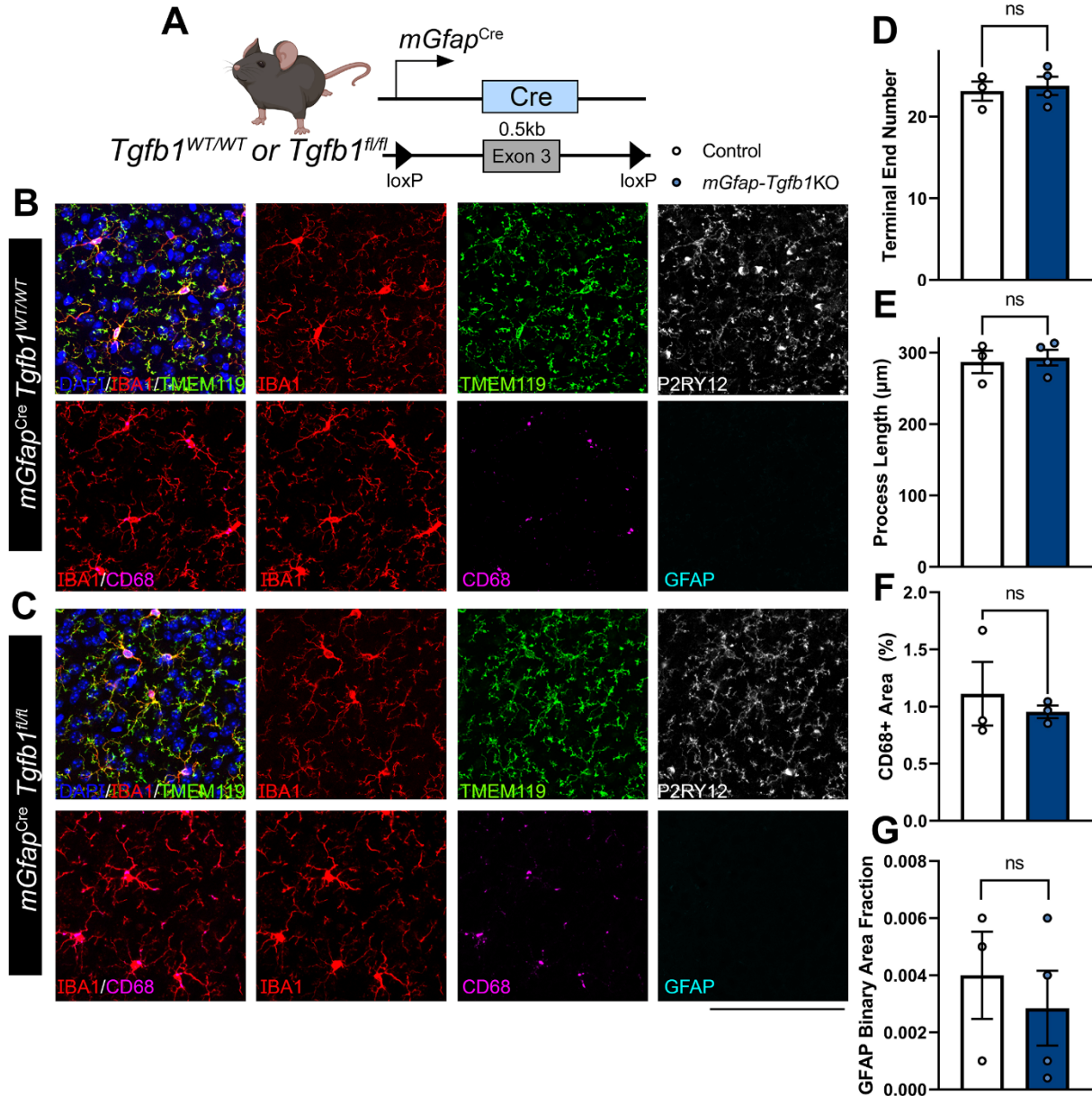
Supplemental Figure 3. Microglia-specific *Tgfb1* gene deletion results in loss of homeostasis of microglia and increase in reactive astrocytes in the hippocampus of the adult mouse brain. (A) Mouse model for targeting microglial *Tgfb1* and timeline. (B) Representative immunohistochemistry images of IBA1, TMEM119, P2RY12, CD68, NeuN, and GFAP in the hippocampus of (C) Control animals, (D) *Cx3cr1*^{CreER(Litt)}*Tgfb1*^{fl/fl} knockouts 5 weeks after tamoxifen administration, and (E) *Cx3cr1*^{CreER(Litt)}*Tgfb1*^{fl/fl} knockouts 8 weeks after tamoxifen administration. Representative results from n=3-5 mice/group, Scale bar = 100µm.



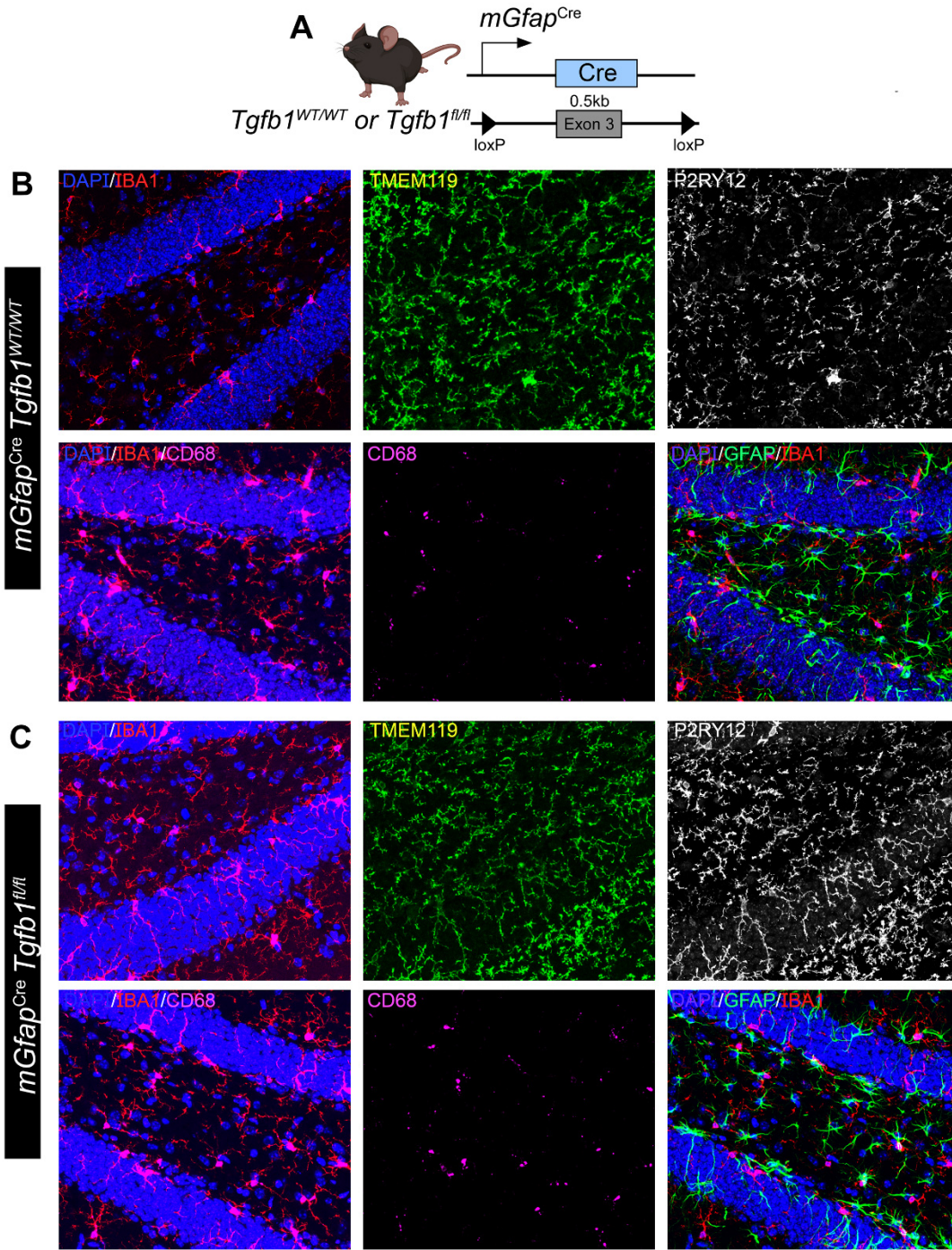
Supplemental Figure 4. Microglia specific *Tgfb1* gene deletion in a second independent *Cx3cr1*^{CreER(Jung)} driver line results in a similar phenotype of loss of homeostasis of microglia and an increase in reactive astrocytes in the cortex of adult mouse brain. (A) Mouse model for targeting microglial *Tgfb1* and timeline. (B-D) Representative images for immunohistochemistry looking at IBA1, TMEM119, P2RY12, CD68, and GFAP in (B) Control *Cx3cr1*^{CreER(Jung)} *Tgfb1*^{wt/wt} + TAM animals, (C) *Cx3cr1*^{CreER(Jung)} *Tgfb1*^{fl/fl} mice + Veh control and (D) *Cx3cr1*^{CreER(Jung)} *Tgfb1*^{fl/fl} mice + TAM at 3 weeks after tamoxifen administration. Representative results from n=3-5 mice/group, Scale bar = 100 μ m.



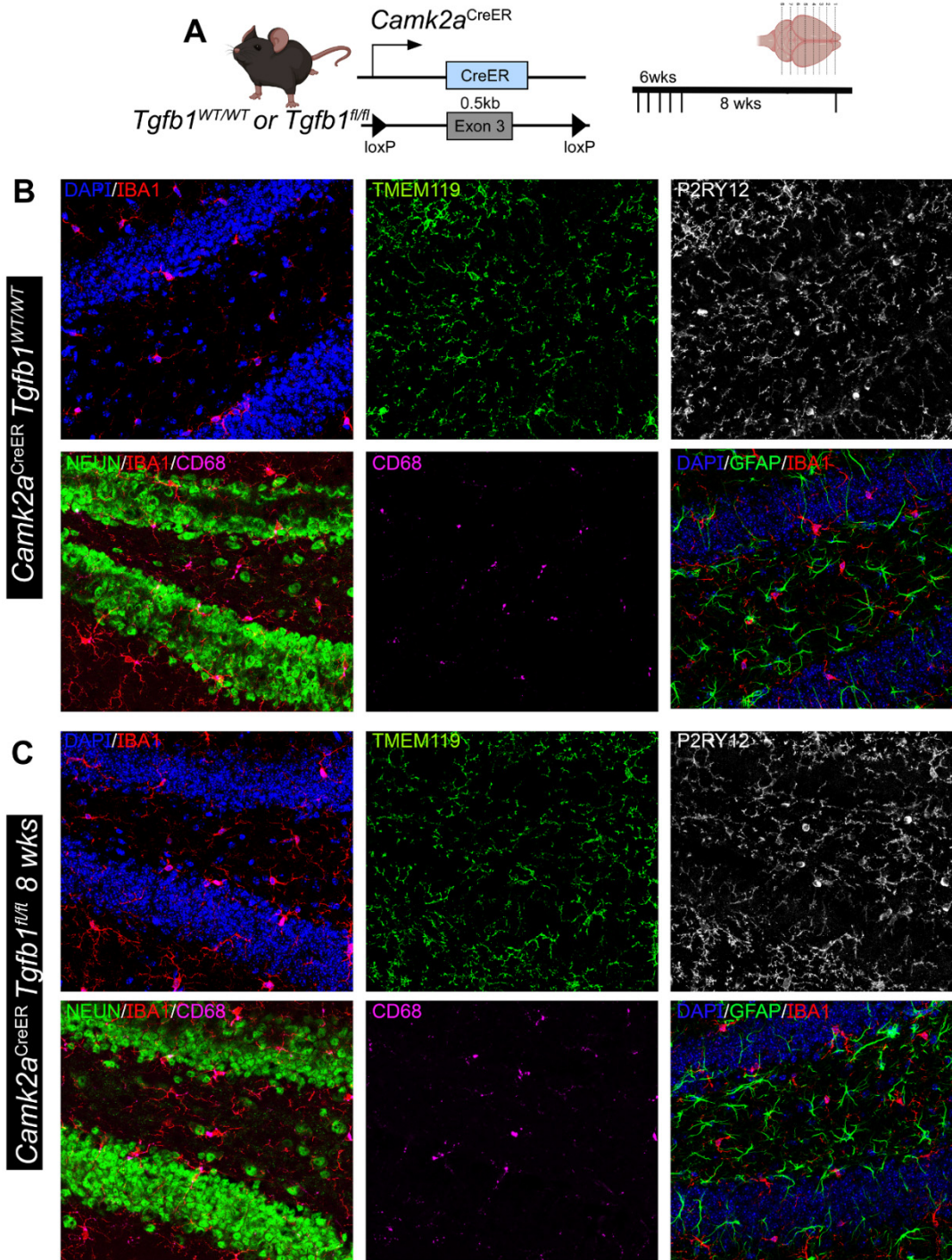
Supplementary Figure 5. Astrocyte-specific *Tgfb1* gene deletion in the *Aldh111^{CreER}* driver does not affect the homeostasis of microglia or GFAP expression in astrocytes in adult mouse brain (hippocampus). (A) Astrocyte iKO mouse model and experimental timeline. (B,C) Representative immunohistochemistry images of hippocampus from TAM treated (8 weeks post) control (B) *Aldh111^{CreER}Tgfb1^{wt/wt}* and (C) iKO *Aldh111^{CreER}Tgfb1^{fl/fl}* tissue showing IBA1, TMEM119, P2RY12, CD68, and GFAP immunostaining. Representative results from n=3-5 mice/group, Scale bar = 100 μ m.



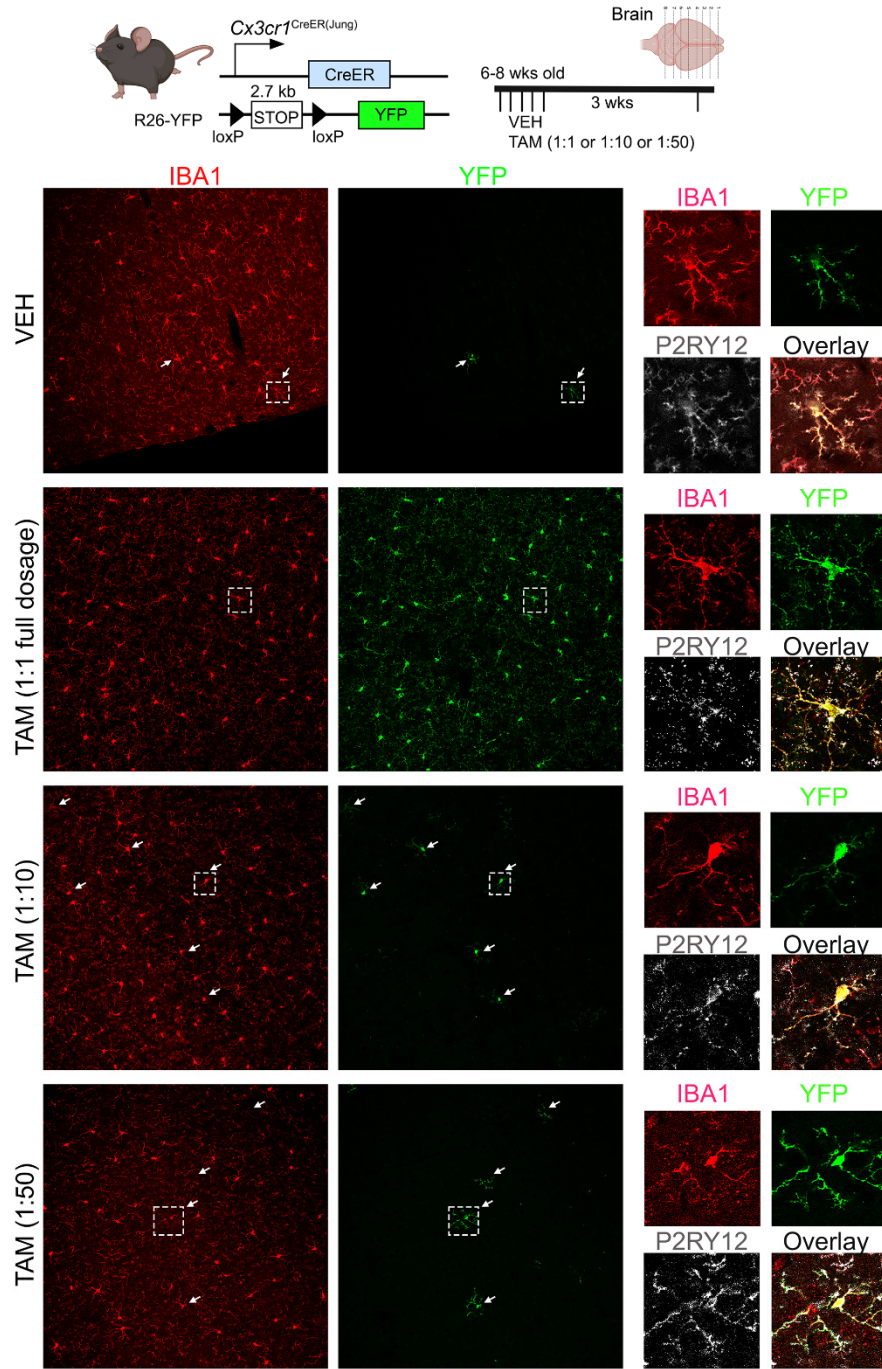
Supplementary Figure 6. Astrocyte-specific *Tgfb1* gene deletion in the perinatal constitutive *mGfap^{Cre}* driver line does not affect the homeostasis of microglia or GFAP expression in astrocytes in adult mouse brain (cortex). (A) Astrocyte constitutive KO mouse model used and experimental timeline. (B,C) Representative images of control *mGfap^{Cre}Tgfb1^{wt/wt}* (B) and cKO *mGfap^{CreER}Tgfb1^{fl/fl}* tissue showing IBA1, TMEM119, P2RY12, CD68, and GFAP immunostaining. Quantification of microglia ramification via (D) terminal end number, (E) process length, and (F) CD68+ immunoreactive % area. (G) Quantification of astrocyte reactivity using GFAP+ immunoreactive area fraction. (control n=3; cKO n=4) ns=not significant. Mean±SE, Scale bar = 100µm.



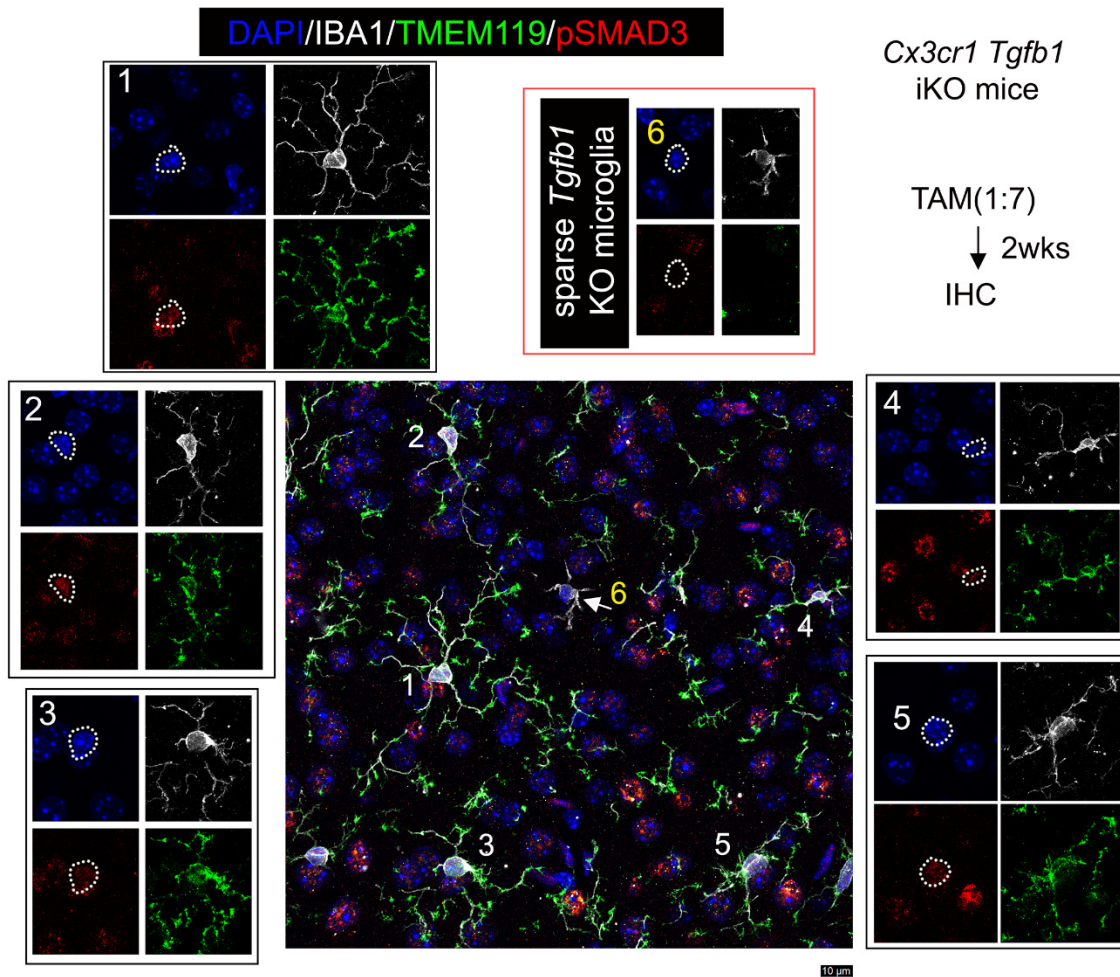
Supplemental Figure 7. Astrocyte-specific *Tgfb1* gene deletion in the perinatal constitutive *mGfap*^{Cre} driver line does not affect the homeostasis of microglia or GFAP expression in astrocytes in the adult mouse brain (hippocampus). (A) Astrocyte constitutive KO mouse model used and experimental timeline. (B, C) Representative images of control *mGfap*^{Cre}*Tgfb1*^{wt/wt} (B) and cKO *mGfap*^{CreER}*Tgfb1*^{fl/fl} tissue showing IBA1, TMEM119, P2RY12, CD68, and GFAP immunostaining. Representative results from n=3-5 mice/group. Scale bar = 100 μ m.



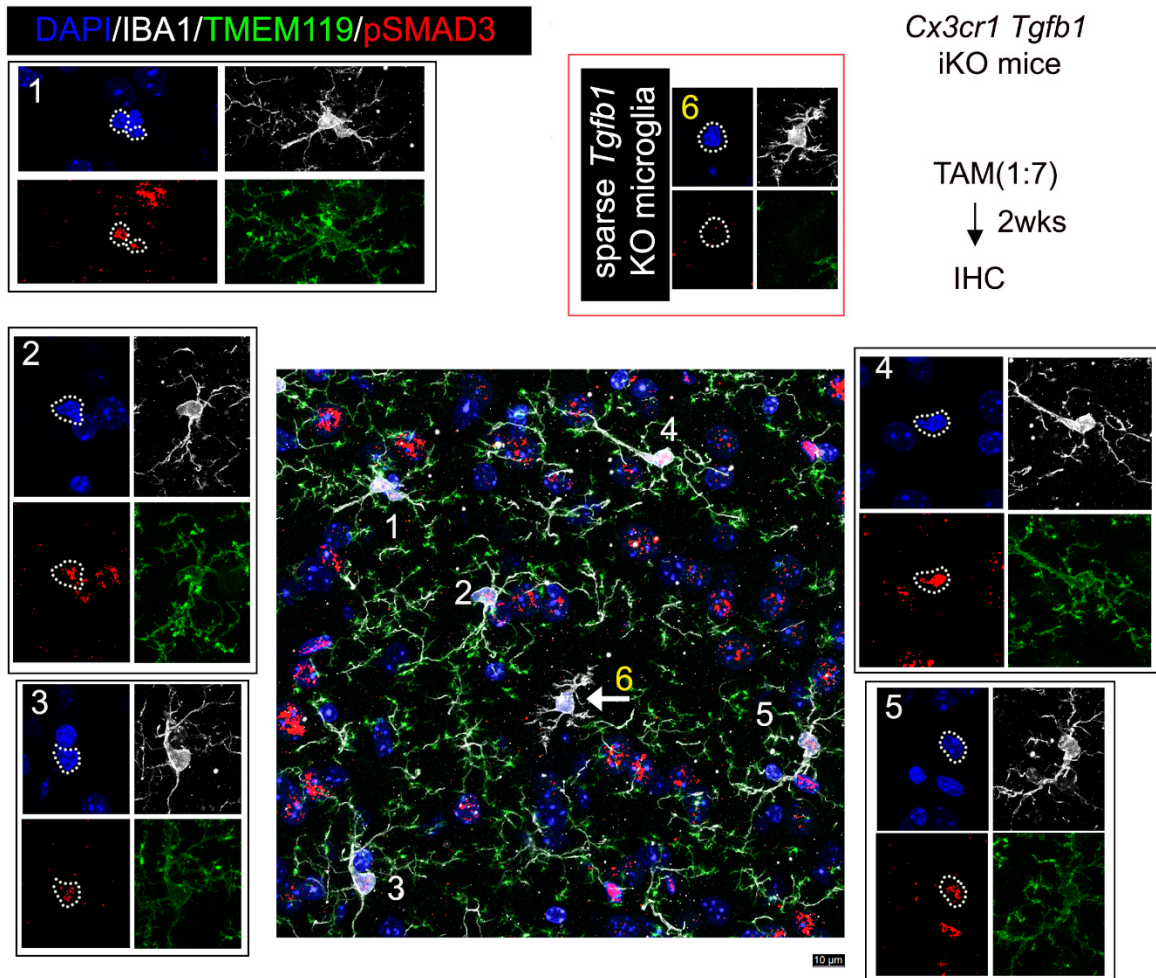
Supplementary Figure 8. Forebrain neuronal specific *Tgfb1* gene deletion in the *Camk2a*^{CreER} driver does not affect the homeostasis of microglia or GFAP expression in astrocytes in the adult mouse brain (hippocampus). (A) Neuron iKO mouse model used and experimental timeline. (B,C) Representative images of control *Camk2a*^{CreER}*Tgfb1*^{wt/wt} (B) and iKO *Camk2a*^{CreER}*Tgfb1*^{fl/fl} tissue showing IBA1, TMEM119, P2RY12, CD68, and GFAP. Representative results from n=3-5 mice/group. Scale bar = 100 μ m.



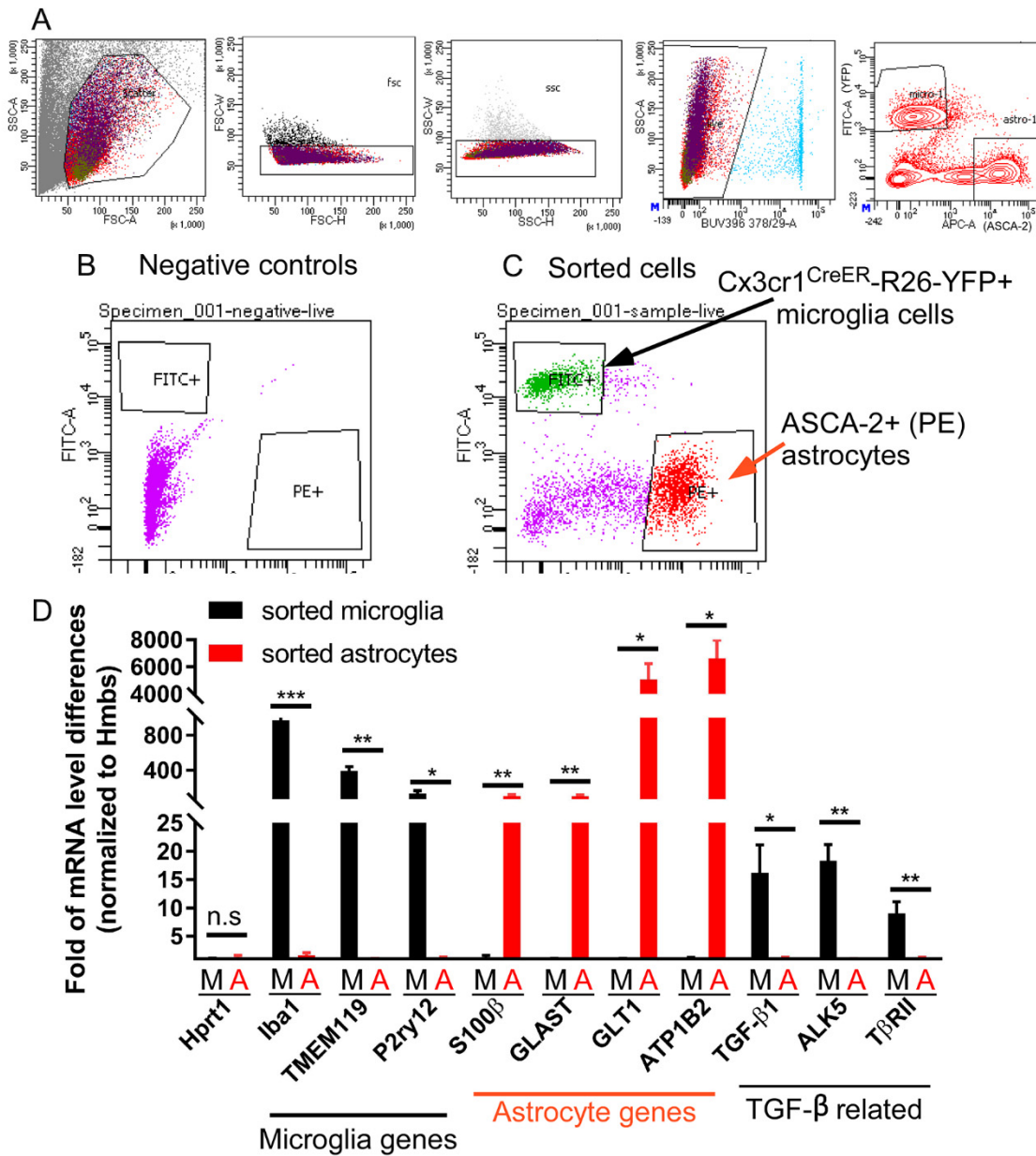
Supplemental Figure 9. Titration of Tamoxifen dosage to enable sparse recombination of a floxed allele in single microglia in adult mouse brain. (A) The reporter mouse model used to test recombination efficiency in floxed reporter allele. (B-E) Representative IHC images showing IBA1, YFP, and P2RY12 labeling from (B) vehicle-treated, (C) full TAM (180mg/kg) dosage, (D) 1:7-1:10 TAM dosage, and (E) 1:50 TAM dosage treated brain tissue. We observed similar recombination efficiency which lead to sparse labeling in individual microglia in 1:7-1:10 TAM dosage in our study. P2RY12 expression indicates that parenchyma microglia are recombined. Representative results from n=3-5 mice/group. Scale Bar = 100 μ m.



Supplemental Figure 10. Additional representative pSMAD3 immunostaining labeling confirms the downregulation of TGF- β downstream signaling in dyshomeostatic individual microglia in the sparse *Tgfb1* iKO model. (A) Mouse model used to examine sparse iKO in microglia and experimental timeline with TAM dosage. (B) Representative image showing co-immunohistochemical staining with DAPI, IBA1, TMEM119, and pSMAD3. (B1-5) Surrounding normal microglia showing TMEM119 expression and pSMAD3 immunostaining. (B6) A single microglia cell with loss of TMEM119 expression and loss of pSMAD3 labeling. White arrow (microglia #6) marks the sparse recombined individual iKO microglia. Representative results from n=3 iKO mice. Scale bar = 10 μ m.

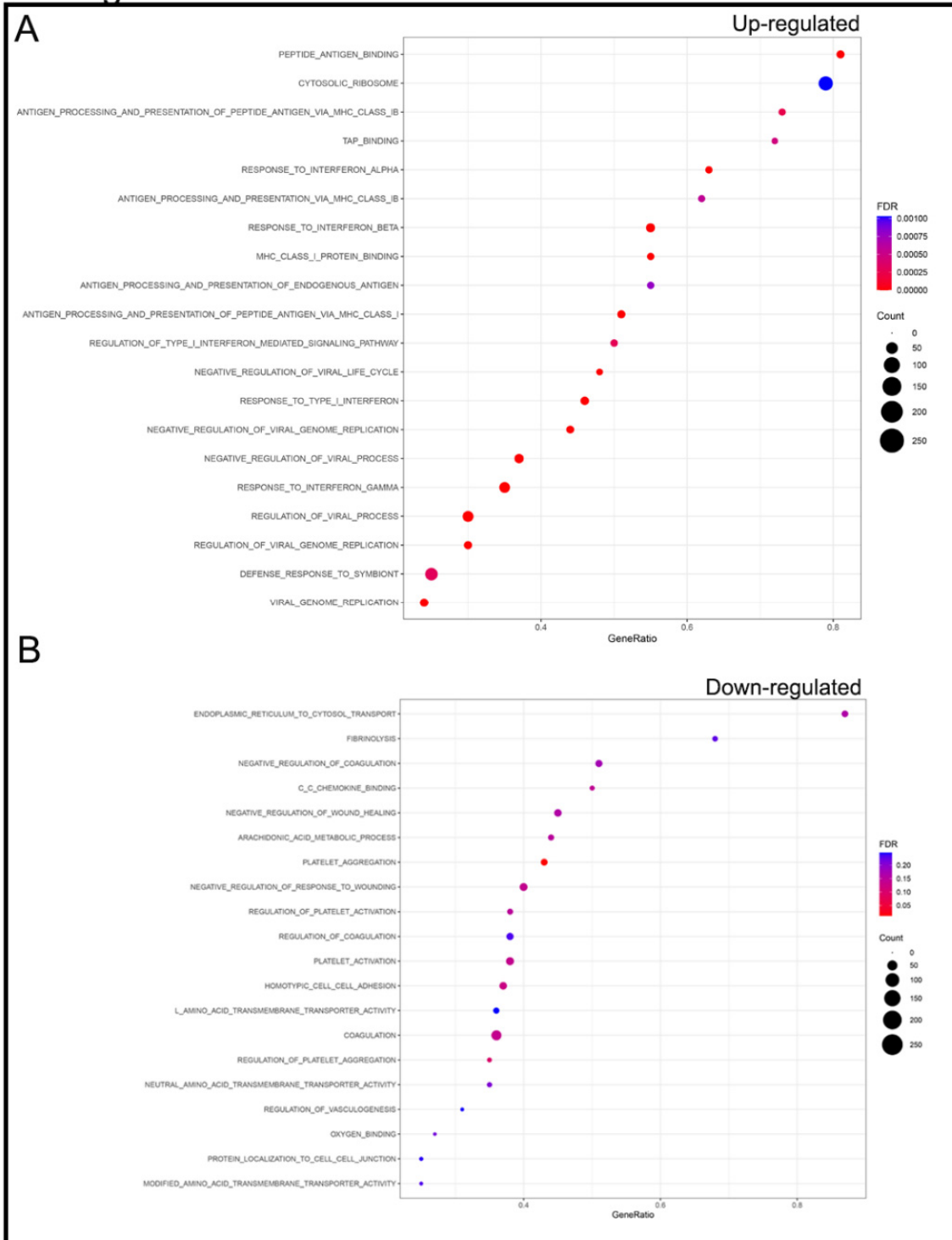


Supplemental Figure 11. Additional representative pSMAD3 immunostaining labeling confirms the downregulation of TGF- β downstream signaling in dyshomeostatic individual microglia in the sparse *Tgfb1* iKO model. (A) Mouse model used to examine sparse iKO in microglia and experimental timeline with TAM dosage. (B) Representative image showing co-immunohistochemical staining with DAPI, IBA1, TMEM119, and pSMAD3. (B1-5) Surrounding normal microglia showing TMEM119 expression and pSMAD3 immunostaining. (B6) A single microglia cell with loss of TMEM119 expression and loss of pSMAD3 labeling. White arrow (microglia #6) marks the sparse recombinant individual iKO microglia. Representative results from n=3 iKO mice. Scale bar = 10 μ m.

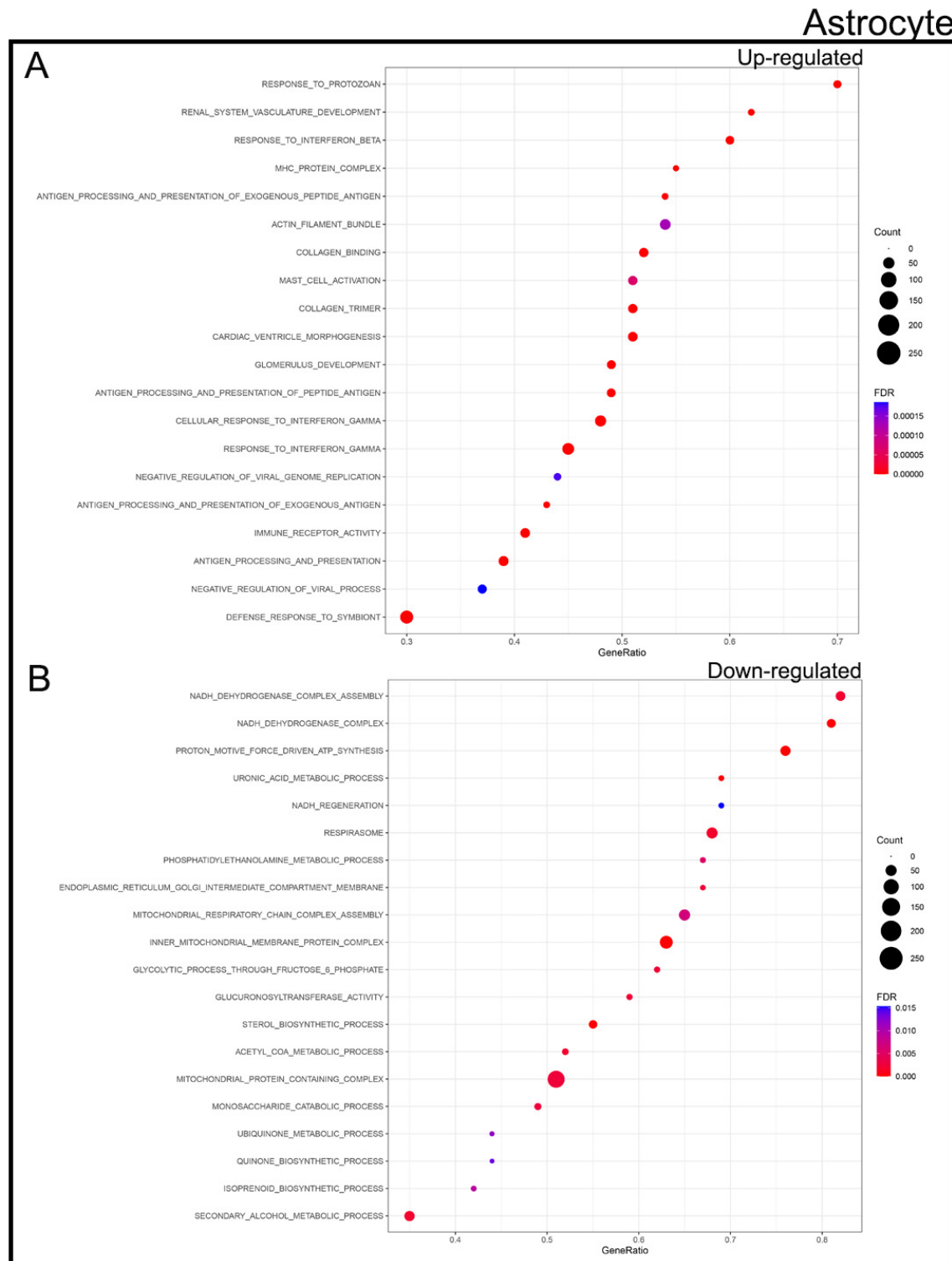


Supplementary Figure 12. Simultaneous sorting of microglia and astrocyte from the same mouse brain and subsequent RNA extraction and qRT-PCR supporting efficient sorting of microglia and astrocytes from the same brain. (A) Gating strategies for isolation of microglia based on TAM-induced R26-YFP expression and ASCA-2 staining on astrocytes. (B) Examples of unstained samples from a non-TAM treated and non-immunostained brain sample (left) and TAM-treated Cx3cr1CreER-R26-YFP mice that is stained with ASCA-2 antibodies. (C) The purity of sorted cells was validated using qRT-PCR by cell type-specific marker expression for microglia and astrocytes respectively. Note that TGFβ1 (ligand) and both type I (ALK5) and type II (TbrII) receptors are substantially enriched in microglia compared to astrocytes. *, **, and *** p < 0.05, 0.01, 0.001. Student's t-test, n=4 brains.

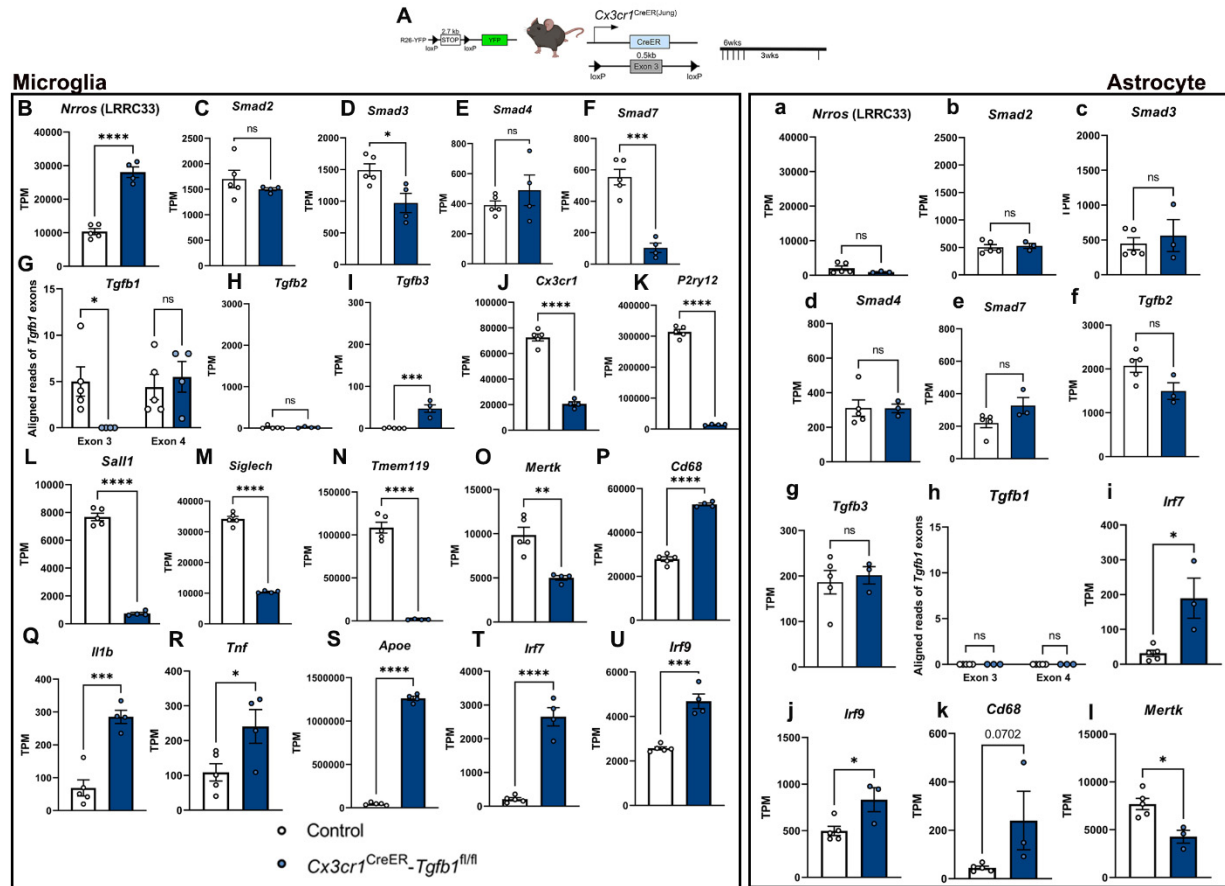
Microglia



Supplementary Figure 13. GSEA Analysis of bulk RNA-sequencing data set examining GO pathways in microglia from *Cx3cr1*^{CreER(Jung)}*Tgfb1*^{fl/fl} compared to controls. (A) Up-regulated and (B) down-regulated GO pathways in brain microglia three weeks after loss of microglial *Tgfb1*.



Supplementary Figure 14. GSEA Analysis of bulk RNA-sequencing data set examining GO pathways in astrocytes from *Cx3cr1*^{CreER(Jung)}*Tgfb1*^{fl/fl} compared to controls. (D) Up-regulated and (E) down-regulated GO pathways of astrocytes from MG-*Tgfb1* iKO mice.



Supplementary Fig 15. Gene expression changes observed in TGF- β signaling pathway component genes, microglia signature genes, and pro-inflammatory genes. (A) Mouse model used. (B-I) Expression levels of TGF- β signaling components in control microglia and MG-*Tgfb1* iKO microglia. (J-O) Expression levels of microglia signature genes and (P-U) pro-inflammatory genes. (a-h) Astrocytic expression of TGF- β signaling pathway components in control and MG-*Tgfb1* iKO astrocytes. (i-l) Differentially expressed pro-inflammatory genes in astrocytes. *, **, *, **** p < 0.05, 0.01, 0.001, 0.0001. Student's t-test, each data point represents a single animal.**